

Article

Bipolar Electrochemical Analysis of Chirality in Complex Media through Miniaturized Stereoselective Light-Emitting Systems

Silvia Cauteruccio ¹, Valentina Pelliccioli ¹, Sara Grecchi ¹, Roberto Cirilli ², Emanuela Licandro ¹ and Serena Arnaboldi ^{1,*}

¹ Dipartimento di Chimica, Università degli Studi di Milano, Via Golgi 19, 20133 Milan, Italy

² Centro Nazionale per il Controllo e la Valutazione dei Farmaci, Istituto Superiore di Sanità, Viale Regina Elena, 299, 00161 Rome, Italy

* Correspondence: serena.arnaboldi@unimi.it; Tel.: +39-(349)-555-3986

Abstract: Environmentally relevant contaminants endowed with chirality may include pharmaceutical compounds, flame retardants, perfluoroalkyl chemicals, pesticides, and polychlorinated biphenyls. Despite having similar physicochemical properties, enantiomers may differ in their biochemical interactions with enzymes, receptors, and other chiral molecules leading to different biological responses. In this work, we have designed a wireless miniaturized stereoselective light-emitting system able to qualitatively detect a chiral contaminant (3,4-dihydroxyphenylalanine, DOPA) dissolved in reduced volumes (in the microliters range), through bipolar electrochemistry. The diastereomeric environment was created by mixing the enantiomers of an inherently chiral inductor endowed with helical shape (7,8-dipropyltetrathia[7]helicene) and the chiral probe (DOPA) in micro-solutions of a commercial ionic liquid. The synergy between the inductor, the applied electric field, and the chiral pollutant was transduced by the light emission produced from a miniaturized light-emitting diode (LED) exploited in such an approach as a bipolar electrode.

Keywords: helical chirality; bipolar electrochemistry; light emitting devices; chiral contaminants; enantioselectivity



Citation: Cauteruccio, S.; Pelliccioli, V.; Grecchi, S.; Cirilli, R.; Licandro, E.; Arnaboldi, S. Bipolar Electrochemical Analysis of Chirality in Complex Media through Miniaturized Stereoselective Light-Emitting Systems. *Chemosensors* **2023**, *11*, 131. <https://doi.org/10.3390/chemosensors11020131>

Academic Editors: Victor Borovkov, Riina Aav, Roberto Paolesse, Manuela Stefanelli and Donato Monti

Received: 20 January 2023

Revised: 7 February 2023

Accepted: 8 February 2023

Published: 13 February 2023



Copyright: © 2023 by the authors. Licensee MDPI, Basel, Switzerland. This article is an open access article distributed under the terms and conditions of the Creative Commons Attribution (CC BY) license (<https://creativecommons.org/licenses/by/4.0/>).

1. Introduction

In Nature proteins, enzymes, amino acids, carbohydrates, nucleosides and a number of alkaloids and hormones are chiral compounds, existing as mirror images, called enantiomers, with the same physicochemical scalar properties. Environmental chiral pollutants have been studied since the 90s. The introduction of new analytical techniques such as gas chromatography (GC), high-performance liquid chromatography (HPLC), and capillary electrophoresis (CE), often coupled to mass spectrometry (MS) and tandem mass spectrometry (MS/MS) for quantification, allowed the detection of their properties. [1]

Persistent organic pollutants (POPs), pesticides, flame retardants, and pharmaceuticals are the most widespread chiral chemicals. Since the enantiomers may have different biological and toxicological effects, it is of great interest to study and understand their environmental behavior. It is well known that the enantiomeric composition is unaffected by physical and chemical processes, and antipodes can be detected just in the case when they interact in a chiral environment.

Screening and monitoring approaches avoid the improper disposal of pollutant solutions improving chiral chemicals management. The analytical techniques listed above have been used to separate the pollutant enantiomers because of their high specificity, selectivity, and sensitivity, but they have shown some limitations such as the requirement of expensive and sophisticated equipment, operational complications, high cost of analysis,

and time-consuming procedures. Moreover, these methods require tedious sample preparation, pretreatment, and pre-concentration protocols, before the analysis of trace-level pollutants in food and environmental samples resulting in unsuitable on-site or on-spot screening [2–11].

In this frame, electrochemical sensing strategies satisfy the desired expectations of the user providing reliability, simplicity, rapid analysis, portability, and low cost, in synergy with their appreciable selectivity, high sensitivity, ease of operation, and compatibility with complex samples [4–15]. In particular electroanalytical techniques allow quantifying the current, charge, phase, potential, and frequency signal outputs associated with chemical/biological/biochemical redox reactions [16–21].

However conventional electrodes and electrochemical set-ups are still rigid, and bulky, and require a relatively large volume of electrolytic solutions, hindering their on-site applications. Recently bipolar electrochemistry (BE) has become an interesting alternative to classic electrochemical set-ups. This approach is completely wireless, and the working electrode, or bipolar electrode (BPE), is remotely placed in the cell where the analytes of interest are collected. Briefly, by applying an electric field (ϵ), between two feeder electrodes, a polarization potential difference (ΔV) is generated at the extremities of a BPE. Commonly chemical transformations (redox reactions) are triggered only when the ΔV overcomes the thermodynamic threshold potential (ΔV_{min}). Indeed, this asymmetric polarization of the BPE generates a current, flowing through it, which is proportional to the concentration of the analytes under study [22–24]. This concept has been successfully used in electrosynthesis, [25,26] photoelectrochemistry [27], and electrochemical sensing. [28,29] Furthermore, this method has been recently coupled with chirality, to detect enantiomers quantitatively and qualitatively in solution via different optical, mechanical, and dynamic read-outs. [30–36] However, in most of these examples, sophisticated BPE designs are required, since at least the chiral inductor has to be deposited asymmetrically on one extremity of the electrode.

Herein we designed a bipolar stereoselective light-emitting system able to qualitatively recognize a chiral contaminant in reduced volumes (in the microliters range), through bipolar electrochemistry. An inherently chiral helical molecule, namely the 7,8-dipropyltetrathia[7]helicene (7-TH-2Pr), is tested as a chiral inductor. Helicenes are inherently chiral molecules composed of *ortho*-annulated benzene or heteroaromatic rings, which assume a nonplanar helix-like structure because of the steric repulsive interaction between the terminal rings [37–40]. The helical structure can be either left- or right-handed, and according to the helicity rule proposed by Cahn, Ingold, and Prelog, [41] a helicene can have either *M* configuration and *P* configuration for left- and right-handed helixes, respectively. Owing to the electronic properties afforded by the π -conjugated system in combination with the chiroptical features provided by their peculiar screw-shaped skeleton, helicenes have been studied in different areas of science, including materials science, macromolecular chemistry, nonlinear optics, nanosciences, stereoselective catalysis, chemical biology, and supramolecular chemistry to name a few [37,38,42]. Nowadays, a plethora of structural modifications of the helicenes has been made to improve their physicochemical and chiroptical properties and provide novel functions. Among them, the introduction of a heterocycle (e.g., pyrrole, pyridine, furan, thiophene, silole, phosphole) in the benzene-based helical skeleton (i.e., carbohelicenes) leads to the class of heterohelicenes, in which the presence of the heteroatom significantly affects the geometric parameters and the electronic structure of the helix [43,44]. In particular, the family of thiahelicenes, formed by condensed thiophene and benzene rings, has attracted considerable attention because of the presence of thiophene rings which confer the peculiar electronic properties of oligothiophenes to the helical skeleton [45–47]. Indeed, thiahelicenes are electron-richer systems than carbohelicenes and have higher conjugation efficiency and electrochemical reactivity [48].

Tetrathia[7]helicenes, in which four thiophene rings alternate with three benzene rings, are a class of configurationally stable thiahelicenes having an extended conjugated π system [49]. The steric hindrance between thiophene terminals leads to a significant

torsion with an energy barrier high enough to allow the molecule to exist as stable *P* and *M* enantiomers even at high temperatures (up to 200 °C) [50]. The tetrathia[7]helicene backbone exhibits several points of interest such as easy and regioselective functionalization of terminal thiophene rings, which can be controlled and driven to afford mono- or disubstituted derivatives, and the possibility of modulating the electron properties through appropriate substitutions in the 7- and 8-positions of the central benzene ring. [49] Moreover, its unique flexibility allows the introduction of substituents with different steric demands resulting in remarkable variations in the dihedral angle of the molecule, though preserving the defining helical structure [49]. All these features make tetrathia[7]helicenes valuable systems, especially for applications in optoelectronics, catalysis, biology, and more recently in chiral electroanalysis. In this context, tetrathia[7]helicenes were used to modify the electrode surface as inherently chiral films, by performing a potentiodynamic electrooligomerization of the corresponding enantiopure monomers. Cyclic voltammetry experiments result in significant potential differences (up to 200 mV) for the enantiomers of three chiral probes, in particular a chiral ferrocenyl derivative, DOPA methyl ester, and tyrosine [51].

In this study, the enantiomers of the 3,4-dihydroxyphenylalanine (DOPA) are used as model chiral contaminants. As a matter of fact, L-DOPA has shown lower toxicity than D-DOPA in different studies. Commonly the higher toxicity that D-DOPA exhibits towards mammalian cells, leads to the use of the opposite enantiomer, L-DOPA, in the treatment of Parkinson's disease. Furthermore, the diastereomeric environment for the enantioselective bipolar test is achieved by mixing in the micro-solutions the enantiomers of an inherently chiral inductor endowed with helical shape and the DOPA analytes. The synergy between the inductor, the applied electric field, and the chiral pollutant is transduced in a straightforward optical readout, i.e., the light emission produced by a miniaturized light-emitting diode (LED).

2. Materials and Methods

2.1. Synthesis

Racemic 7,8-dipropyltetrathia[7]helicene ((±)-7-TH-2Pr) was synthesized following the published methodology [52].

2.2. Enantioselective HPLC

HPLC-grade solvents were supplied by Aldrich (Milan, Italy). HPLC enantioseparations were carried out by using stainless-steel Chiralpak[®] IA 250 mm × 4.6 mm, 5 μm, and Chiralpak[®] IA 250 mm × 10 mm, 5 μm, columns (Chiral Technologies Europe, Illkirch-Graffenstaden, France). The analytical HPLC apparatus consisted of a PerkinElmer 200 LC pump equipped with a Rheodyne injector, a 100 μL sample loop, an HPLC Dionex CC-100 oven, and a Jasco Model CD 2095 Plus UV/CD detector. For semi-preparative resolutions, a PerkinElmer 200 LC pump equipped with a Rheodyne injector, a 2 mL sample loop, a PerkinElmer LC 101 oven, and Waters 484 detector was employed. The signal was acquired and processed by the Clarity software of DataApex.

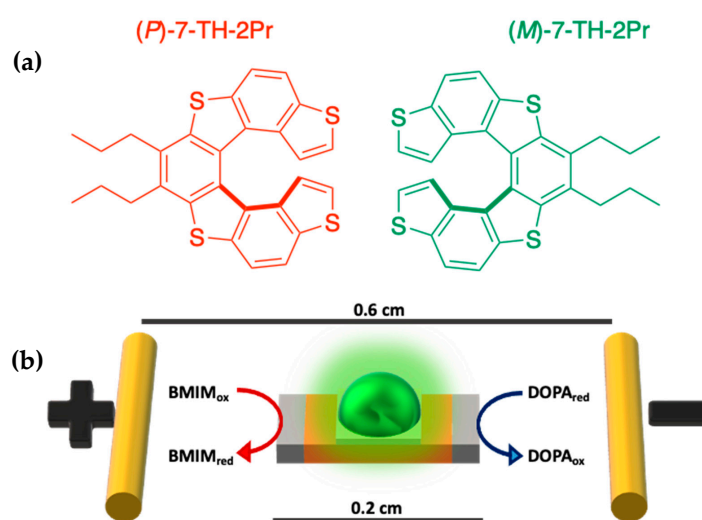
2.3. Circular Dichroism

The circular dichroism spectra of the enantiomers of 7-TH and 7-TH-2Pr were recorded in chloroform at 25 °C by using a Jasco Model J-700 spectropolarimeter. The optical path was 1 mm. The spectra are averagedly computed over four instrumental scans and the intensities are presented in terms of ellipticity values (mdeg).

2.4. Electrochemistry

Au wires (d = 0.25 mm, Alfa Aesar, Haverhill, MA, USA, 99.9%), L- and D- 3,4-dihydroxyphenylalanine (Aldrich, St. Louis, MO, USA, ≥95%), 1-butyl-3-methylimidazolium bis(trifluoro-methylsulfonyl)imide (BMIMtfsi, Aldrich, ≥98%) and miniaturized green light-emitting diodes (LED, 0603 SMD diode, OSRAM Opto Semiconductors, Regensburg,

Germany, 1.70 mm × 0.8 mm) were used as received. Electrochemical characterizations were performed in a 50 μ L droplet of an ionic liquid (IL) solution containing 10 mM (*P*)- or (*M*)-7-TH-2Pr (Scheme 1a) in the presence of 20 mM D-DOPA. Differential pulse voltammetry (DPV) measurements were performed by means of a PalmSense4 potentiostat connected to a personal computer. For the voltammetric measurements, screen-printed electrodes (SPEs, BVT Technologies, WE: carbon, CE: carbon; RE: Ag | AgCl) was used as a miniaturized electrochemical cell. For the bipolar recognition, the light-emitting diode was placed at the center of a glass slide, between two Au feeder electrodes separated by 0.6 cm. Light-emitting bipolar recognition was carried out in 50 μ L of an ionic liquid solution containing 10 mM of (*P*)- or (*M*)-7-TH-2Pr in the presence of 20 mM D- or L-DOPA. Experiments were monitored by using a charge-coupled device (CCD) camera (CANON EOS 70D, Objective Canon Macro Lens 100 mm 1:2.8). Images were processed with ImageJ software.



Scheme 1. (a) Chemical structures of the enantiomers of the 7,8-dipropyl-tetrathia[7]helicene ((*P*)- or (*M*)-7-TH-2Pr). (b) Set-up used for the stereoselective recognition together with the redox reactions associated with the enantioselection process. The BPE is represented by the green LED in the middle that is emitting light according to diastereomeric interactions occurring in the mixture in which it is dipped. Feeder electrodes are the gold wires at the two sides of the scheme.

3. Results

3.1. HLC Separation and Absolute Configuration Assignment of the Enantiomers of 7-TH-2Pr

To develop enantioselective conditions capable of separating the enantiomers of 7-TH-2Pr on an analytical scale, the Chiralpak IA was selected as a chiral stationary phase (CSP) and used in combination with normal-phase *n*-hexane-dichloromethane eluents. This specific experimental design is due to two main reasons: (i) the Chiralpak IA CSP has shown a good chiral recognition ability to the analog 7-TH devoid of two propyl chains [51]; (ii) the presence of dichloromethane as a cosolvent ensures an appreciable solubility of the sample in the mobile phase. In this regard, it is important to emphasize that in the Chiralpak IA CSP, the amylose tris(3,5-dimethylphenylcarbamate) selector is immobilized onto 5 μ m silica particles. The anchoring procedure onto the silica matrix guarantees universal solvent compatibility of the chromatographic chiral packing material and allows the use of medium polarity solvents such as dichloromethane without causing the dissolution of the polymer selector. The best resolution was obtained employing the mixture *n*-hexane–dichloromethane 100:5 (*v/v*) as a mobile phase at a column temperature of 5 $^{\circ}$ C. Under these conditions, the baseline separation of two enantiomers resolution was achieved within 10 min (Figure 1).

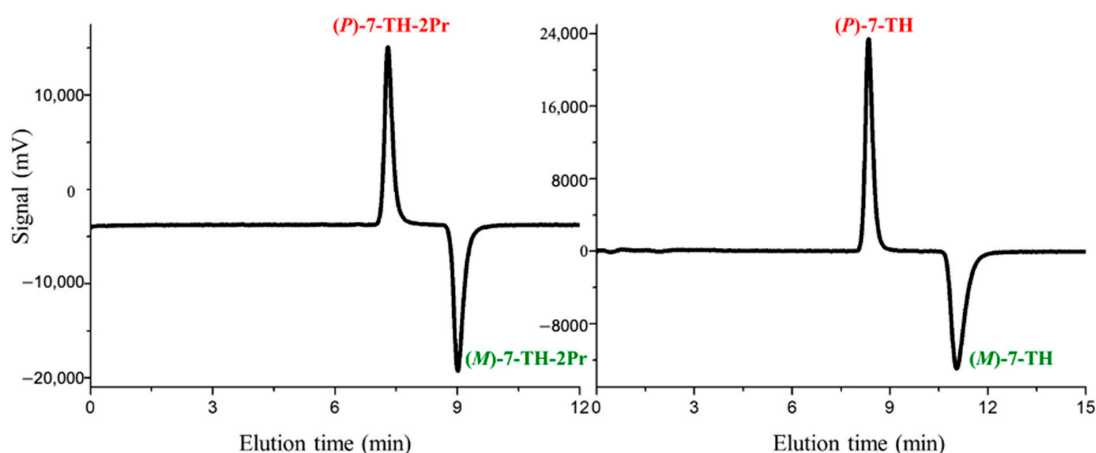


Figure 1. HPLC separation of enantiomers of 7-TH and 7-TH-2Pr on the Chiralpak IA CSP. Chromatographic conditions: column, Chiralpak IA (250 mm × 4.6 mm, 5 μm); mobile phase, n-hexane/dichloromethane 100:5 (v/v); temperature, 5 °C; flow rate, 1 mL/min; detection, CD at 325 nm.

In the successive step, the enantiomer separation was scaled up on a semipreparative scale by using a 250 mm × 10 mm Chiralpak IA column. The sample solution was prepared by dissolving 25 mg of racemate in 1.5 mL of dichloromethane and adding 8.5 mL of n-hexane. The injection volume for a single chromatographic run was 0.5 mL which corresponds to 1.3 mg of chiral sample. By setting the flow rate at 5.0 mL min⁻¹, the enantiomers were collected with a high enantiomeric excess (ee > 99%) and yielded approximately 85% in a time scale similar to the analytical conditions. Assignment of the absolute configuration to the enantiomers collected at the semipreparative level was empirically established by circular dichroism correlation, using the enantiomers of 7-TH as references to known stereochemistry [53,54]. As shown in Figure 2, sharing the same π-conjugated[7]helicene scaffold the enantiomers of the two chiral compounds exhibit intense and very similar electronic CD spectra in chloroform solution. This is indicative that the first eluted enantiomers of both chiral compounds have a P configuration and the more retained one's M configuration. Notably, at the diagnostic wavelength of 325 nm, it exists a univocal correlation between the online CD peak sign acquired during HPLC enantioseparation (Figure 1) and absolute configuration (i.e., the positive online CD peak is attributable to the P enantiomer and vice versa).

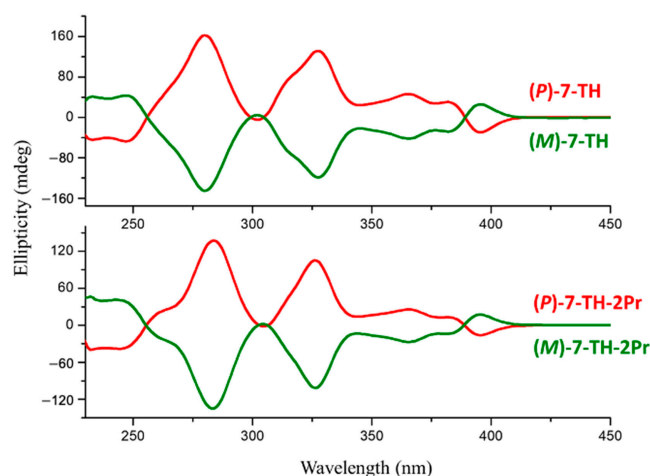


Figure 2. CD spectra of the first eluted (red line) and second eluted (green line) enantiomers of 7-TH and 7-TH-2Pr in chloroform solution.

3.2. Bipolar Stereoselective Recognition

The experimental set-up designed for the stereoselective recognition of the chiral contaminant is displayed in Scheme 1b. Two gold wires, placed at a distance of 0.6 cm, were used as feeder electrodes, whereas a miniaturized green light-emitting diode (0.2 cm length) was used as a BPE. Light emitting systems have gained considerable attention, due to the easy and straightforward visualization of chemical information [55–59]. In particular, light-emitting diodes (LEDs) present the main advantage that light emission can be triggered by the proper coupling of redox reactions at the anode and cathode of the device. Thus, chemical information is encoded on the electric current passing through the LED. In this frame, the use of light emission as a straightforward tool for the possible transduction of chiral information is of great interest. For example, Salinas et al. designed a hybrid polymer microelectronic device modified with intrinsically chiral oligomers, for the wireless transduction of chiral information [33,34]. However, this approach requires the physicochemical modification of one or both poles of the LED, by the direct contact of its extremity with a surface-modified electrode. Such handmade devices lead to electric connection problems which hinder the flow of electrons, triggered by the redox reactions, from the anode to the cathode of the device. To avoid such a limitation, in this work we take advantage of the possible enantioselection capability of chiral inductors dissolved in solution.

In particular, the enantiomers of a helically shaped inherently chiral thia[7]helicene derivative functionalized with two propyl chains in 7 and 8 positions were used as chiral inductors in the solution (Scheme 1a).

At first, to test the effective enantioselection capability of the chiral inductor endowed with a helical shape, voltammetric enantioselection experiments were carried out. Such potentiodynamic measurements were performed by dissolving the enantiopure inductors in an achiral commercial ionic liquid (BMIMtfsi) with the enantiomers of the chiral pollutant (L- or D-DOPA), and by spreading a droplet of the mixture on SPEs. As can be seen from Figure 3a, the (P)- and (M)- helicene, tested towards D-DOPA, show a peak-to-peak separation of 100 mV between the two enantiomers of the helical inductors. This means that, potentially, it is possible to oxidize only one of the DOPA antipodes, by applying a specific potential in the presence of the helicene endowed with the favorable configuration, which induces the stereospecific reaction. Such difference in thermodynamic potential value is based on the induction of a chiral electrode/electrolyte interphase. Since in the presence of an electric field, the helical chiral inductor enables the reorganization of the ionic liquid, the electron transfer takes place in a highly ordered chiral electrode interface. Thus, the oxidation of the chiral analyte is favored only in the proper diastereomeric environment.

After this set of experiments, we evaluated the electric field required to switch on the LED, in the presence of the pristine ionic liquid and a mixture of the IL + L- or D-DOPA, separately. As stated above, the LED was placed at the center of a glass slice between two Au feeder electrodes (Scheme 1b). Afterward, a droplet of the corresponding solution was spread between the feeder electrodes, to guarantee the electrical connection between the two poles of the BPE and the Au wires. Theoretically, when a high enough electric field is applied in such a setup, the BPE gets sufficiently polarized to induce redox reactions at each extremity of the LED.

Based on the principles of BE, the electric field value can be calculated by Equation (1).

$$\varepsilon = \Delta E/L \quad (1)$$

where ΔE is the applied difference of potential and L is the distance between the feeder electrodes. Such ε value is intimately related to the oxidation and reduction potential values of the analytes in solution (E_{ox} and E_{red} , respectively) and the size of the BPE (l), as established in Equation (2).

$$\varepsilon = \Delta V/l = E_{ox} - E_{red}/l \quad (2)$$

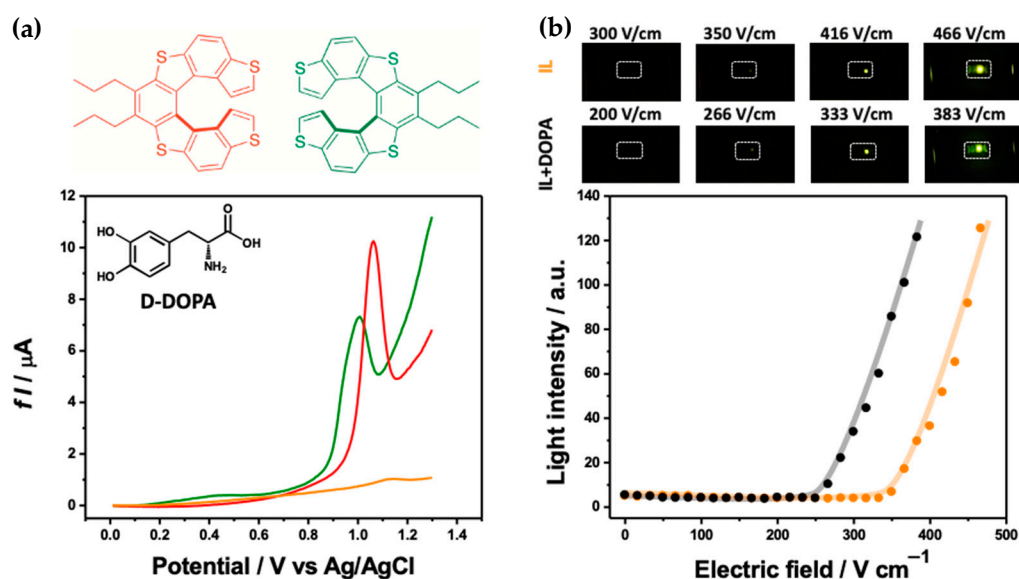


Figure 3. (a) Enantioselection DPV tests carried out on screen-printed cells by dissolving the (*P*)- and (*M*)-chiral inductors (red and green lines, respectively) with 20 mM D-DOPA in a drop of ionic liquid. The orange line stands for the pristine ionic liquid measured in the same operative conditions. (b) On the top: optical pictures at different applied electric fields, indicated in the figure, for the devices tested in the presence of pristine IL (first row) and with IL + 20 mM D-DOPA (second row). On the bottom: maximum light intensity as a function of the applied electric field for the same devices tested in the presence of the pristine IL (orange dots) and with the IL + 20 mM D-DOPA (black dots).

Considering that L and l are constant along all the experiments (0.6 cm and 0.2 cm, respectively), any variation of the applied electric field is directly related to the physico-chemical properties of the analytes in the solution.

As can be seen at electric fields below 200 V cm^{-1} no light emission is produced in both experiments (Figure 3b). However, above 250 V cm^{-1} the oxidation and reduction of DOPA and the IL, respectively, take place, with the concomitant light emission (Figure 3b black dots). For the experiment carried out only with the pristine ionic liquid, electric field values above 350 V cm^{-1} are required to trigger the light emission. In this case, it is possible to assume that the oxidation of the BMIM⁺ cation and the reduction of the tfsi⁻ anion are the induced redox reactions. Thus, the presence of the chiral analyte (i.e., DOPA) shifts to lower electric fields the thermodynamic threshold value required to switch on the LED. Since the reduction of the BMIM⁺ cation is the same in both cases, such differentiation in the absence of the chiral inductor is caused by the lower oxidation potential value of DOPA in comparison to the tfsi⁻ anion.

Finally, after the evaluation of the threshold electric field value, the enantiomeric discrimination by means of the wireless light-emitting device was studied. To test such proof-of-concept, four independent mixtures containing the ionic liquid, one of the enantiomers of DOPA, and one of the enantiomers of the helical inductor were prepared. For each of the four experiments, a droplet of the correspondent mixture was spread on the hand-made bipolar electrochemical cell and the threshold electric field was evaluated. In this case, the triggered redox reactions that occur at the extremities of the LED are (i) the oxidation of DOPA and (ii) the reduction of the IL cation (Scheme 1b).

Theoretically, the presence of the chiral inductor, i.e., the chiral helicene, enables the enantioselective oxidation of a chiral probe. As mentioned above, this is due to the energetically favorable interaction between the chiral inductor and the analyte, which results in a difference in oxidation potential between the enantiomers of the chiral probe. Thus, according to Equation (2), a shift of the threshold electric field to lower values is expected when the chiral analyte oxidizes in the proper diastereomeric environment. As can be seen from Figure 4a, when the (*M*)-chiral inductor is present in the mixture of ionic

liquid and D-DOPA, the threshold electric field required to trigger the light emission is 220 V cm^{-1} ; whereas in the presence of the chiral inductor with the opposite configuration, the potential shifts to higher values (above 280 V cm^{-1}). The specular behavior was obtained with L-DOPA since its oxidation is energetically favored by the (*P*)-chiral inductor (200 V cm^{-1} , Figure 4b).

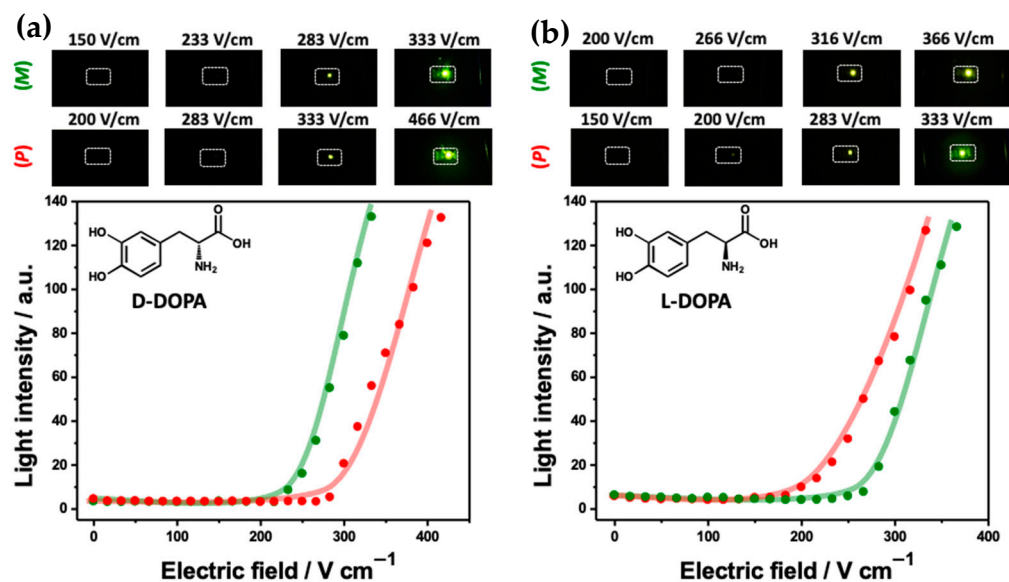


Figure 4. On the top: Optical pictures of the stereoselective devices at different applied electric fields, indicated in the figure, in the presence of (a) D- or (b) L-DOPA, respectively. The readout time for all the experiments is 20 s. On the bottom: maximum light intensity as a function of the applied electric field for two independent devices dipped in mixtures containing (a) 20-mM D-DOPA and (b) 20 mM L-DOPA dissolved in BMIMtfsi ionic liquid in the presence of (*P*)- and (*M*)-7-TH-2Pr chiral inductors (red and green dots, respectively).

4. Discussion

Bipolar electrochemistry is presented as a powerful tool for the transduction of chemical information in solution. As it was demonstrated, a small peak-to-peak separation of 100 mV obtained by conventional electrochemistry, can be enhanced by two orders of magnitude with this wireless approach (difference of threshold electric field around 60 V cm^{-1} or 30 V estimated by Equation (1)). This presents an important advantage when using this concept in enantiomeric mixtures, allowing to obtain well defined individual transduction signals. In the present work, an ionic liquid was chosen as solvent due to its relatively high viscosity, in synergy with the efficient solvent capability, which allows it to work in droplets containing relatively small concentrations of the chiral inductors. Nonetheless, it is important to highlight, that due to the relatively high conductivity of the IL, [58] high electric field values are required to trigger the asymmetrical polarization of the LED, in comparison with aqueous systems. However, it has been demonstrated that an electrified interface can extend the supramolecular order of the ionic liquids [60–64]. In fact, the use of simple ILs, like BMIMtfsi, has shown self-assembling in the presence of an applied electric field. In this specific case, the helical chiral inductor can reorganize the ionic liquid interface when the electric field is applied, inducing a chiral environment. Thus, the electron transfer, associated with the redox processes, takes place in a highly ordered chiral interface. In this context, the electric field differences associated with the oxidation of L- or D-DOPA in the presence of the (*P*)- or (*M*)-chiral inductors, are intimately related to the electron transfers occurring in the proper diastereomeric environment. Furthermore, the above results are the first application of the synergy between bipolar electrochemistry and chiral inductors directly dissolved in solution. Thus, the possible quantitative analysis of

different chiral probes by means of this wireless bipolar light-emitting approach is currently under investigation.

5. Conclusions

In conclusion, miniaturized LEDs have been used for a straightforward optical read-out of chiral information based on bipolar electrochemistry. The novelty of the present approach compared to previous ones [33,34] is that the chiral inductors are directly dissolved in solution instead to be electrodeposited on a conductor connected to the anode of the LED. Thus, this approach is based on the synergy between the diastereomeric environment, formed by the ionic liquid and the chiral inductor, and the proper enantiomer dissolved in the solution. Furthermore, the wireless light emission can be modulated by the applied electric field to selectively oxidize only one of the enantiomers. In addition, with this setup, it is possible to work with microcells where only a few microliters of the solution containing the analytes are required to guarantee contact between the LED and the feeder electrodes. Furthermore, the light intensity of the device is found to be directly related to the intrinsic chirality of the system. Finally, the electrochemical characterization and the evaluation of the enantioselective capability of alternative chiral inductors in different media, rather than ionic liquids, will open up novel applications in the field of chiral recognition. Therefore, the presented approach opens up an alternative and complementary strategy for chiral discrimination with respect to more conventional electrochemical and spectroscopic methods.

Author Contributions: S.A. and S.C. conceptualization, S.A. project administration, investigation, data curation, writing-original draft preparation, review and editing, V.P. and S.C. synthesis, review and editing, R.C. enantioselective HPLC and circular dichroism, review and editing, E.L. and S.G. review and editing. All authors have read and agreed to the published version of the manuscript.

Funding: This work has been funded by the H2020 European Research Council (ERC) under the HORIZON-ERC-2021 work program (grant agreement no 101040798, ERC Starting grant CHEIR).

Institutional Review Board Statement: Not applicable.

Informed Consent Statement: Not applicable.

Data Availability Statement: Not applicable.

Acknowledgments: SA is grateful to A. Kuhn and G. Salinas for the fruitful scientific discussions.

Conflicts of Interest: The authors declare no conflict of interest.

References

1. Wong, C.S.; Elmayergi, B.H. Chiral Environmental Contaminants. In *Encyclopedia of Analytical Chemistry*; John Wiley & Sons, Ltd.: Hoboken, NJ, USA, 2009; pp. 1–25.
2. Xia, N.; Wang, Q.; Liu, L. Nanomaterials-Based Optical Techniques for the Detection of Acetylcholinesterase and Pesticides. *Sensors* **2014**, *15*, 499–514. [[CrossRef](#)]
3. Zhao, F.; Wu, J.; Ying, Y.; She, Y.; Wang, J.; Ping, J. Carbon nanomaterial-enabled pesticide biosensors: Design strategy, biosensing mechanism, and practical application. *Trends Anal. Chem.* **2018**, *106*, 62–83. [[CrossRef](#)]
4. Cheng, W.; Tang, X.; Zhang, Y.; Wu, D.; Yang, W. Applications of metal-organic framework (MOF)-based sensors for food safety: Enhancing mechanisms and recent advances. *Trends Food Sci. Technol.* **2021**, *112*, 268–282. [[CrossRef](#)]
5. Zhang, C.; Jiang, C.; Lan, L.; Ping, J.; Ye, Z.; Ying, Y. Nanomaterial-based biosensors for agro-product safety. *Trends Anal. Chem.* **2021**, *143*, 116369. [[CrossRef](#)]
6. Raghavan, V.S.; O'Driscoll, B.; Bloor, J.M.; Li, B.; Katare, P.; Sethi, J.; Gorothi, S.S.; Jenkins, D. Emerging graphene-based sensors for the detection of food adulterants and toxicants—A review. *Food Chem.* **2021**, *355*, 129547. [[CrossRef](#)] [[PubMed](#)]
7. Tajik, S.; Beitollahi, H.; Nejad, F.G.; Dourandish, Z.; Khalilzadeh, M.A.; Jang, H.W.; Venditti, R.A.; Varma, R.S.; Shokouhimehr, M. Recent Developments in Polymer Nanocomposite-Based Electrochemical Sensors for Detecting Environmental Pollutants. *Ind. Eng. Chem. Res.* **2021**, *60*, 1112–1136. [[CrossRef](#)] [[PubMed](#)]
8. Pérez-Fernández, B.; Costa-García, A.; De La Escosura-Muñiz, A. Electrochemical (Bio) Sensors for Pesticides Detection Using Screen-Printed Electrodes. *Biosensors* **2020**, *10*, 32. [[CrossRef](#)]
9. Narenderan, S.T.; Meyyanathan, S.N.; Babu, B. Review of pesticide residue analysis in fruits and vegetables. Pre-treatment, extraction and detection techniques. *Food Res. Int.* **2020**, *133*, 109141. [[CrossRef](#)]

10. Tajik, S.; Orooji, Y.; Ghazanfari, Z.; Karimi, F.; Beitollahi, H.; Varma, R.S.; Jang, H.W.; Shokouhimehr, M. Nanomaterials modified electrodes for electrochemical detection of Sudan I in food. *J. Food Meas. Charact.* **2021**, *15*, 3837–3852. [[CrossRef](#)]
11. Shahid, M.K.; Kashif, A.; Fuwad, A.; Choi, Y. Current advances in treatment technologies for removal of emerging contaminants from water—A critical review. *Coord. Chem. Rev.* **2021**, *442*, 213993. [[CrossRef](#)]
12. Siwal, S.S.; Zhang, Q.; Saini, A.K.; Gupta, V.K.; Roberts, D.; Saini, V.; Coulon, F.; Pareek, B.; Thakur, V.K. Recent advances in bio-electrochemical system analysis in biorefineries. *J. Environ. Chem. Eng.* **2021**, *9*, 105982. [[CrossRef](#)]
13. Sudhaik, A.; Raizada, P.; Thakur, S.; Saini, R.V.; Saini, A.K.; Singh, P.; Kumar Thakur, V.; Nguyen, V.H.; Khan, A.A.P.; Asiri, A.M. Synergistic photocatalytic mitigation of imidacloprid pesticide and antibacterial activity using carbon nanotube decorated phosphorus doped graphitic carbon nitride photocatalyst. *J. Taiwan Inst. Chem. Eng.* **2020**, *113*, 142–154. [[CrossRef](#)]
14. Prakash, J.; Parveen, A.; Mishra, Y.K.; Kaushik, A. Nanotechnology-assisted liquid crystals-based biosensors: Towards fundamental to advanced applications. *Biosens. Bioelectron.* **2020**, *168*, 112562. [[CrossRef](#)] [[PubMed](#)]
15. García-Miranda Ferrari, A.; Rowley-Neale, S.J.; Banks, C.E. Screen-printed electrodes: Transitioning the laboratory in-to-the field. *Talanta Open.* **2021**, *3*, 100032. [[CrossRef](#)]
16. Tajik, S.; Beitollahi, H.; Garkani Nejad, F.; Sheikhshoae, I.; Nugraha, A.S.; Jang, H.W.; Yamauchi, Y.; Shokouhimehr, M. Performance of metal-organic frameworks in the electrochemical sensing of environmental pollutants. *J. Mater. Chem. A* **2021**, *9*, 8195–8220. [[CrossRef](#)]
17. Vikrant, K.; Tsang, D.C.W.; Raza, N.; Giri, B.S.; Kukkar, D.; Kim, K.H. Potential Utility of Metal-Organic Framework-Based Platform for Sensing Pesticides. *ACS Appl. Mater. Interfaces* **2018**, *10*, 8797–8817. [[CrossRef](#)] [[PubMed](#)]
18. Ranjith, K.S.; Vilian, A.T.E.; Ghoreishian, S.M.; Umaphathi, R.; Huh, Y.S.; Han, Y.K. An ultrasensitive electrochemical sensing platform for rapid detection of rutin with a hybridized 2D–1D MXene-FeWO₄ nanocomposite. *Sens. Actuators B Chem.* **2021**, *344*, 130202. [[CrossRef](#)]
19. Ezhil Vilian, A.T.; Umaphathi, R.; Hwang, S.K.; Lee, M.J.; Huh, Y.S.; Han, Y.K. Simple synthesis of a clew-like tungsten carbide nanocomposite decorated with gold nanoparticles for the ultrasensitive detection of tert-butylhydroquinone. *Food Chem.* **2021**, *348*, 128936. [[CrossRef](#)]
20. Vilian, A.T.E.; Umaphathi, R.; Hwang, S.K.; Huh, Y.S.; Han, Y.K. Pd–Cu nanospheres supported on Mo₂C for the electrochemical sensing of nitrites. *J. Hazard. Mater.* **2021**, *408*, 124914. [[CrossRef](#)]
21. Vilian, A.T.E.; Ranjith, K.S.; Lee, S.J.; Hwang, S.K.; Umaphathi, R.; Oh, C.W.; Huh, Y.S.; Han, Y.K. Controllable synthesis of bottlebrush-like ZnO nanowires decorated on carbon nanofibers as an efficient electrocatalyst for the highly sensitive detection of silymarin in biological samples. *Sens. Actuators B Chem.* **2020**, *321*, 128544. [[CrossRef](#)]
22. Salinas, G.; Arnaboldi, S.; Bouffier, L.; Kuhn, A. Recent advances in bipolar electrochemistry with conducting polymers. *ChemElectroChem* **2022**, *9*, e202101234. [[CrossRef](#)]
23. Shida, N.; Zhou, Y.; Inagi, S. Bipolar electrochemistry: Powerful tool for electrifying functional material synthesis. *Acc. Chem. Res.* **2019**, *52*, 2598–2608. [[CrossRef](#)] [[PubMed](#)]
24. Rahn, K.L.; Anand, R.K. Recent advancements in bipolar electrochemistry methods of analysis. *Anal. Chem.* **2021**, *93*, 103–123. [[CrossRef](#)]
25. Zhang, C.; Zhang, H.; Pi, J.; Zhang, L.; Kuhn, A. Bulk electrocatalytic NADH cofactor regeneration with bipolar electrochemistry. *Angew. Chem. Int. Ed.* **2022**, *61*, e202111804. [[CrossRef](#)] [[PubMed](#)]
26. Ketkaew, M.; Assavapanumat, S.; Klinyod, S.; Kuhn, A.; Wattanakit, C. Bifunctional Pt/Au Janus electrocatalysis for simultaneous oxidation/reduction of furfural with bipolar electrochemistry. *Chem. Commun.* **2022**, *58*, 4312–4315. [[CrossRef](#)] [[PubMed](#)]
27. Loget, G.; Li, G.; Fabre, B. Logic gates operated by bipolar photoelectrochemical water splitting. *Chem. Commun.* **2015**, *51*, 1115–1118. [[CrossRef](#)]
28. Anand, R.K.; Johnson, E.S.; Chui, D.T. Negative dielectrophoretic capture and repulsion of single cells at a bipolar electrode: The impact of faradaic ion enrichment and depletion. *J. Am. Chem. Soc.* **2015**, *137*, 776–783. [[CrossRef](#)]
29. Wu, S.; Zhou, Z.; Xu, L.; Su, B.; Fang, Q. Integrating bipolar electrochemistry and electrochemiluminescence imaging with microdroplets for chemical analysis. *Biosens. Bioelectron.* **2014**, *53*, 148–153. [[CrossRef](#)]
30. Salinas, G.; Niamlaem, M.; Kuhn, A.; Arnaboldi, S. Recent advances in Electrochemical transduction of chiral information. *Curr. Opin. Colloid Interface Sci.* **2022**, *6*, 101626. [[CrossRef](#)]
31. Arnaboldi, S.; Gupta, B.; Benincori, T.; Bonetti, G.; Cirilli, R.; Kuhn, A. Absolute chiral recognition with hybrid wireless electrochemical actuators. *Anal. Chem.* **2020**, *92*, 10042–10047. [[CrossRef](#)]
32. Arnaboldi, S.; Salinas, G.; Bonetti, G.; Cirilli, R.; Benincori, T.; Kuhn, A. Bipolar electrochemical measurements of enantiomeric excess with inherently chiral polymer actuators. *ACS Meas. Au* **2021**, *1*, 110–116. [[CrossRef](#)]
33. Salinas, G.; Arnaboldi, S.; Bonetti, G.; Cirilli, R.; Benincori, T.; Kuhn, A. Hybrid light-emitting devices for the straightforward readout of chiral information. *Chirality* **2021**, *33*, 875–882. [[CrossRef](#)]
34. Salinas, G.; Bonetti, G.; Cirilli, R.; Benincori, T.; Kuhn, A.; Arnaboldi, S. Wireless light-emitting device for the determination of chirality in real samples. *Electrochim. Acta* **2022**, *421*, 140494. [[CrossRef](#)]
35. Arnaboldi, S.; Salinas, G.; Karajic, A.; Garrigue, P.; Benincori, T.; Bonetti, G.; Cirilli, R.; Bichon, S.; Gounel, S.; Mano, N.; et al. Direct dynamic read-out of molecular chirality with autonomous enzyme-driven swimmers. *Nat. Chem.* **2021**, *13*, 1241–1247. [[CrossRef](#)]

36. Arnaboldi, S.; Salinas, G.; Bonetti, G.; Cirilli, R.; Benincori, T.; Kuhn, A. Bipolar electrochemical rotors for the direct transduction of molecular chiral information. *Biosens. Bioelectron.* **2022**, *218*, 114740. [[CrossRef](#)] [[PubMed](#)]
37. Chen, C.-F.; Shen, Y. *Helicene Chemistry, from Synthesis to Applications*; Springer: Berlin/Heidelberg, Germany, 2017. [[CrossRef](#)]
38. Shen, Y.; Chen, C.-F. Helicenes: Synthesis and Applications. *Chem. Rev.* **2012**, *112*, 1463–1535. [[CrossRef](#)] [[PubMed](#)]
39. Gingras, M. One hundred years of helicene chemistry. Part 1: Non-stereoselective syntheses of carbohelicenes. *Chem. Soc. Rev.* **2013**, *42*, 968–1006. [[CrossRef](#)]
40. Gingras, M.; Félix, G.; Peresutti, R. One hundred years of helicene chemistry. Part 2: Stereoselective syntheses and chiral separations of carbohelicenes. *Chem. Soc. Rev.* **2013**, *42*, 1007–1050. [[CrossRef](#)] [[PubMed](#)]
41. Cahn, R.S.; Ingold, C.; Prelog, V. Specification of Molecular Chirality. *Angew. Chem. Int. Ed.* **1966**, *5*, 385–415. [[CrossRef](#)]
42. Gingras, M. One hundred years of helicene chemistry. Part 3: Applications and properties of carbohelicenes. *Chem. Soc. Rev.* **2013**, *42*, 1051–1095. [[CrossRef](#)]
43. Dhbaibi, K.; Favereau, L.; Crassous, J. Enantioenriched Helicenes and Helicenoids Containing Main-Group Elements (B, Si, N, P). *Chem. Rev.* **2019**, *119*, 8846–8953. [[CrossRef](#)]
44. Pop, F.; Zigon, N.; Avarvari, N. Main-Group-Based Electro- and Photoactive Chiral Materials. *Chem. Rev.* **2019**, *119*, 8435–8478. [[CrossRef](#)]
45. Licandro, E.; Cauteruccio, S.; Dova, D. Thiahelicenes: From basic knowledge to applications. In *Advances in Heterocyclic Chemistry*; Ramsden, C.A., Scriven, E.F.V., Eds.; Elsevier: Amsterdam, The Netherlands, 2016; Volume 118, pp. 1–46. [[CrossRef](#)]
46. Hoffmann, N. Photochemical reactions applied to the synthesis of helicenes and helicene-like compounds. *J. Photochem. Photobiol. C* **2014**, *19*, 1–19. [[CrossRef](#)]
47. Collins, S.K.; Vachon, M.P. Unlocking the potential of thiaheterohelicenes: Chemical synthesis as the key. *Org. Biomol. Chem.* **2006**, *4*, 2518–2524. [[CrossRef](#)]
48. Bossi, A.; Falciola, L.; Graiff, C.; Maiorana, S.; Rigamonti, C.; Tiripicchio, A.; Licandro, E.; Mussini, P.R. Electrochemical activity of thiahelicenes: Structure effects and electrooligomerization ability. *Electrochim. Acta* **2009**, *54*, 5083–5097. [[CrossRef](#)]
49. Cauteruccio, S.; Dreuw, A.; Licandro, E.; Mussini, P.R. Tetrathiahelicenes: An infinite source of inspiration. In *Helicenes: Synthesis, Properties and Applications*; Crassous, J., Stará, I.G., Starý, I., Eds.; Wiley: Hoboken, NJ, USA, 2022. [[CrossRef](#)]
50. Yamada, K.; Nakagawa, H.; Kawazura, H. Thermal racemization of thiaheterohelicenes. *Bull. Chem. Soc. Jpn.* **1986**, *59*, 2429–2432. [[CrossRef](#)]
51. Arnaboldi, S.; Cauteruccio, S.; Grecchi, S.; Benincori, T.; Marcaccio, M.; Orbelli Biroli, A.; Longhi, G.; Licandro, E.; Mussini, P.R. Thiahelicene-based inherently chiral films for enantioselective electroanalysis. *Chem. Sci.* **2019**, *10*, 1539–1548. [[CrossRef](#)]
52. Licandro, E.; Rigamonti, C.; Ticozzelli, M.T.; Monteforte, M.; Baldoli, C.; Giannini, C.; Maiorana, S. Synthesis and functionalization of novel tetrathia[7]helicenes as new push-pull systems. *Synthesis* **2006**, *21*, 3670–3678. [[CrossRef](#)]
53. Kawasaki, T.; Suzuki, K.; Licandro, E.; Bossi, A.; Maiorana, S.; Soai, K. Enantioselective synthesis induced by tetrathia[7]helicenes in conjunction with asymmetric autocatalysis. *Tetrahedron Asymmetry* **2006**, *17*, 2050–2053. [[CrossRef](#)]
54. Nakagawa, H.; Obata, A.; Yamada, K.; Kawazura, H. Crystal and molecular structures of tetrathia[7]heterohelicene: Racemate and enantiomer. *J. Chem. Soc. Perkin Trans.* **1985**, *2*, 1899–1903. [[CrossRef](#)]
55. Salinas, G.; Pavel, I.A.; Sojic, N.; Kuhn, A. Electrochemistry-based light-emitting mobile systems. *ChemElectroChem* **2020**, *7*, 4853–4862. [[CrossRef](#)]
56. Salinas, G.; Dauphin, A.L.; Colin, C.; Villani, E.; Arbault, S.; Bouffier, L.; Kuhn, A. Chemo- and magnetotaxis of self-propelled light-emitting chemo-electronic swimmers. *Angew. Chem. Int. Ed.* **2020**, *59*, 7508–7513. [[CrossRef](#)]
57. Salinas, G.; Beladi-Mousavi, S.M.; Gerasimova, L.; Bouffier, L.; Kuhn, A. Wireless imaging of transient redox activity based on bipolar light-emitting electrode arrays. *Anal. Chem.* **2022**, *94*, 14317–14321. [[CrossRef](#)]
58. Zhao, Y.; Bouffier, L.; Xu, G.; Loget, G.; Sojic, N. Electrochemiluminescence with semiconductor (nano) materials. *Chem. Sci.* **2022**, *13*, 2528–2550. [[CrossRef](#)]
59. Meng, C.; Knežević, S.; Du, F.; Guan, Y.; Kanoufi, F.; Sojic, N.; Xu, G. Recent advances in electrochemiluminescence imaging analysis. *eScience* **2022**, *2*, 591–605. [[CrossRef](#)]
60. Fu, Y.; Cui, X.; Zhang, Y.; Feng, T.; He, J.; Zhang, X.; Bai, X.; Cheng, Q. Measurement and correlation of the electrical conductivity of the ionic liquid [BIMIM][TFSI] in binary organic solvents. *J. Chem. Eng. Data* **2018**, *63*, 1180–1189. [[CrossRef](#)]
61. Perkin, S.; Crowhurst, L.; Niedermeyer, H.; Welton, T.; Smith, A.M.; Goswami, N.N. Self-assembly in the electrical double layer of ionic liquids. *Chem. Commun.* **2011**, *47*, 6572–6574. [[CrossRef](#)]
62. Ivanistsev, V.; O'Connor, S.; Fedorov, M.V. Poly(a)morphic portrait of the electrical double layer in ionic liquids. *Electrochem. Commun.* **2014**, *48*, 61–64. [[CrossRef](#)]
63. Matsushita, S.; Yan, B.; Yamamoto, S.; Jeong, Y.S.; Akagi, K. Synthesis of Helical Polyacetylene in Chiral Nematic Liquid Crystals Using Crown Ether Type Binaphthyl Derivatives as Chiral Dopants. *J. Am. Chem. Soc.* **2005**, *127*, 14647–14654. [[CrossRef](#)]
64. Rizzo, S.; Arnaboldi, S.; Mihali, V.; Cirilli, R.; Forni, A.; Gennaro, A.; Isse, A.A.; Pierini, M.; Mussini, P.R.; Sannicolò, F. "Inherently Chiral" Ionic-Liquid Media: Effective Chiral Electroanalysis on Achiral Electrodes. *Angew. Chem.* **2017**, *129*, 2079–2082. [[CrossRef](#)]

Disclaimer/Publisher's Note: The statements, opinions and data contained in all publications are solely those of the individual author(s) and contributor(s) and not of MDPI and/or the editor(s). MDPI and/or the editor(s) disclaim responsibility for any injury to people or property resulting from any ideas, methods, instructions or products referred to in the content.